




## Article

# Functionalization of an Alginate-Based Material by Oxidation and Reductive Amination

Ronny G. Huamani-Palomino <sup>1,\*</sup> , Bryan M. Córdova <sup>1</sup>, Elvis Renzo Pichilingue L. <sup>2</sup> , Tiago Venâncio <sup>3</sup> and Ana C. Valderrama <sup>1,\*</sup> 

<sup>1</sup> Laboratorio de Investigación en Biopolímeros y Metalofármacos, Facultad de Ciencias, Escuela Profesional de Química, Universidad Nacional de Ingeniería, Av. Túpac Amaru 210, Lima 15333, Peru; bcordovav@uni.pe

<sup>2</sup> Facultad de Ciencias, Escuela de Química, Universidad Nacional de Ingeniería. Av. Túpac Amaru 210, Lima 15333, Peru; epichilinguel@uni.pe

<sup>3</sup> Laboratório de Ressonância Magnética Nuclear, Departamento de Química, Universidade Federal de São Carlos, São Carlos 13565-905, São Paulo, Brazil; venancio@ufscar.br

\* Correspondence: rohuamanip@uni.pe (R.G.H.-P.); ana.valderrama.n@uni.edu.pe (A.C.V.)

**Abstract:** This research focused on the synthesis of a functional alginate-based material via chemical modification processes with two steps: oxidation and reductive amination. In previous alginate functionalization with a target molecule such as cysteine, the starting material was purified and characterized by UV-Vis, <sup>1</sup>H-NMR and HSQC. Additionally, the application of FT-IR techniques during each step of alginate functionalization was very useful, since new bands and spiked signals around the pyranose ring (1200–1000 cm<sup>-1</sup>) and anomeric region (1000–750 cm<sup>-1</sup>) region were identified by a second derivative. Additionally, the presence of C<sub>1</sub>-H<sub>1</sub> of β-D-mannuronic acid residue as well as C<sub>1</sub>-H<sub>1</sub> of α-L-guluronic acid residue was observed in the FT-IR spectra, including a band at 858 cm<sup>-1</sup> with characteristics of the N-H moiety from cysteine. The possibility of attaching cysteine molecules to an alginate backbone by oxidation and post-reductive amination processes was confirmed through <sup>13</sup>C-NMR in solid state; a new peak at 99.2 ppm was observed, owing to a hemiacetal group formed in oxidation alginate. Further, the peak at 31.2 ppm demonstrates the presence of carbon -CH<sub>2</sub>-SH in functionalized alginate—clear evidence that cysteine was successfully attached to the alginate backbone, with 185 μmol of thiol groups per gram polymer estimated in alginate-based material by UV-Visible. Finally, it was observed that guluronic acid residue of alginate are preferentially more affected than mannuronic acid residue in the functionalization.

**Keywords:** alginate; functionalization; oxidation; reductive amination



**Citation:** Huamani-Palomino, R.G.; Córdova, B.M.; Pichilingue L., E.R.; Venâncio, T.; Valderrama, A.C. Functionalization of an Alginate-Based Material by Oxidation and Reductive Amination. *Polymers* **2021**, *13*, 255. <https://doi.org/10.3390/polym13020255>

Received: 1 December 2020

Accepted: 5 January 2021

Published: 14 January 2021

**Publisher's Note:** MDPI stays neutral with regard to jurisdictional claims in published maps and institutional affiliations.



**Copyright:** © 2021 by the authors. Licensee MDPI, Basel, Switzerland. This article is an open access article distributed under the terms and conditions of the Creative Commons Attribution (CC BY) license (<https://creativecommons.org/licenses/by/4.0/>).

## 1. Introduction

The past decade has seen an increase in the importance of the utilization of algal-based materials and improvement of the physicochemical properties of polysaccharides extracted from the cell wall of brown algae (Figure 1) [1]. This is due to the strong dependence on taxonomic characteristics and the effect of environmental growing conditions on natural sources, which effect its metabolites' properties [2–5]. Depending on the type of seaweed, time of harvest, temperature, and other factors, metabolites with novel features can be obtained. These have been used in a wide range of applications [1]. For instance, phlorotannins present in brown seaweeds have been applied as a bioactive agent for their antioxidant, bactericidal and inhibitive properties [6]. Also, the anticoagulant and elicitor properties of fucoidan obtained from brown seaweed have demonstrated promising applications in biomedical fields [7]. Other polysaccharides like alginate have been gaining attention for their application in biomedical and environmental fields [8,9].

Alginate is a linear anionic copolymer composed of [1–4] β-D-mannuronic' acid (M) and α-L-guluronic acid (G). This polysaccharide is mainly extracted from brown seaweeds

and is characterized by its random block distribution, which offers unique properties depending on the length of the polymeric chain and the presence of different stretches of alternating or homogeneous M and G sequences, referred to as MG-blocks, MM-blocks or GG-blocks. The M/G ratio is an important parameter that gives crucial information associated with the block composition of alginates from a particular brown seaweed. It must be mentioned that the block distribution depends exclusively on the species, habitat, season of harvest and salinity of water [10,11]. Thus, it is essential to refer to the algae's background for chemical modification purposes.

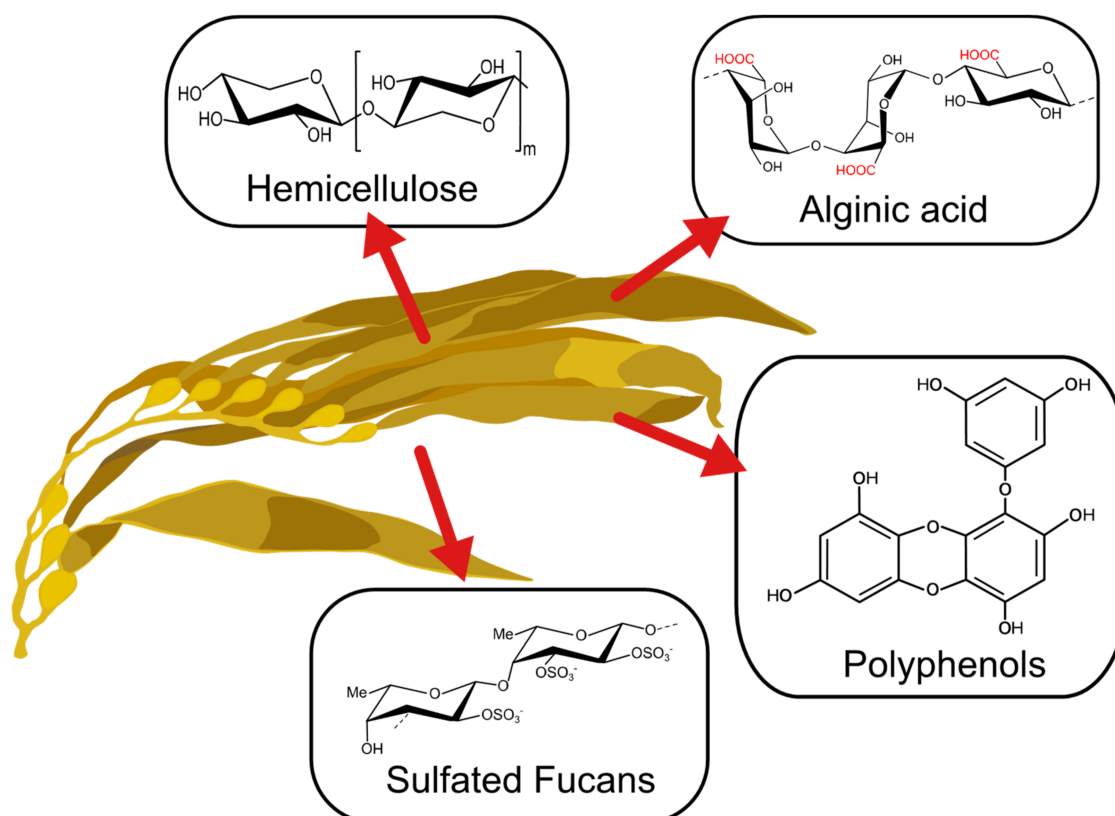


**Figure 1.** Main compounds present in brown seaweed.

Alginates are employed industrially for their viscosifying properties, water binding capacities and gelling properties [12], which correlate with the amount of GG blocks in the polymer chain as well as the presence of divalent cations in the aqueous medium [13]. These properties have allowed us to widen alginate applications, especially in biomedical areas, including wound healing [14–16], cell microencapsulation [17–19] and drug delivery systems [20–22]. However, the main limitation regarding these applications lies especially on low biocompatibility and poor mechanical properties, preventing the utilization of unmodified alginates for sophisticated biomedical areas such as cell immobilization [23,24]. Taking into account these drawbacks, functionalization of alginate-based materials emerges as an excellent option to enhance the quality and long-term stability of alginates without restricting the action of some specific properties characteristic of them [25]. Furthermore, the physical properties of alginate-based materials can be improved while avoiding the incorporation of other materials, such as carbon nanomaterials [26,27] or nanocellulose [28]. Different studies have reported that chelating [29], permeation [30] and, especially, mucoadhesive [31,32] properties can be improved when sulphur-containing molecules are attached to the alginate backbone. In particular, the synthesis of thiol-containing biopolymers offers numerous attractive features for a variety of biomedical applications in which the biomaterial can perform as a drug delivery system and bioadhesive [33,34].

In this regard, Bernkop-Schnürch et al. synthesized thiomers from the implantation of thiol groups in different polysaccharides, such as chitosan, pectin and alginate [23,35,36]. The main pathway to obtain thiomers in alginate is to render the carboxylic acid group into an amine-reactive reagent via carbodiimide coupling [31,37], but the main drawback is that this procedure tends to generate side products during the functionalization process [37,38]. On the other hand, other chemical routes that involve oxidation and reductive amination processes [39,40] have shown promising properties, including increasing the degradability and chain flexibility of the polymer [41,42]. Novel materials obtained have demonstrated their versatility in varied fields, but most of these are not focused on structural changes upon oxidation and subsequent grafting. Based on this, the present study aims to provide an efficient method to functionalize the alginate in two steps via oxidation and post reductive amination reaction for evaluating the preference of uronic residue involved in this process.

## 2. Materials and Methods

### 2.1. Materials

Commercial-grade sodium alginate ( $M_w = 124.2$ ,  $M_n = 57.8$  and  $PI = 2.1$  (Table S1) obtained by SEC-MALS (Figure S1)) and L-cysteine hydrochloride ( $\text{HSCH}_2\text{CH}(\text{NH}_2)\text{COOH}\cdot\text{HCl}$ ) were obtained from Sigma Aldrich Chemistry (St. Louis, MO, USA). All other reagents were supplied by Merck (KGaA, Darmstadt, Germany) except for ethylene glycol (98%, Fermont).

### 2.2. Purification of Commercial Alginate

The alginate (Alg) was purified in order to remove polyphenol compounds that are usually present in commercial-grade products. For this purpose, a solution of 1% was treated with n-butanol in a ratio of 3 to 2. This mixture was sonicated for 1 h, and then the solution was reposed until the formation of 2 phases. Finally, the aqueous phase was separated by decantation and lyophilized for 24 h to obtain the purified alginate (AlgP).

### 2.3. Functionalization of Purified Alginate with Cysteine

The functionalization of AlgP with cysteine was prepared following the procedure reported by our group previously, but with several modifications [32]. First, 4 g of AlgP was dissolved thoroughly in 170 mL of distilled water prior the addition of  $0.2 \text{ mol L}^{-1}$   $\text{NaIO}_4$  (30 mL). This solution was stirred for 6 h in complete darkness to prevent undesired reactions [43]. Then, 1 mL of ethylene glycol was added and stirred for 30 min under the same conditions. The solution containing the oxidized alginate was dialyzed against deionized water by using a cellulose membrane (cut-off molecular weight of 12 kDa) until the conductivity of the aqueous medium was less than  $10 \mu\text{S cm}^{-1}$ . Next, the oxidized alginate (AlgPO) was obtained by freeze-drying for 36 h. Afterward, 40 mL of  $0.1 \text{ mol L}^{-1}$  phosphate buffer solution (PBS, pH 7.4) was used as the medium to dissolve 0.4 g of AlgPO before the addition of  $0.2 \text{ mol L}^{-1}$  cysteine solution (10 mL). Finally, the mixture was stirred for 24 h at room temperature prior to the addition of  $0.05 \text{ mol L}^{-1}$   $\text{NaBH}_4$  (10 mL). The solution reacted for 12 h and a functionalized alginate-based material (AlgPOS) was obtained through precipitation in ethanol and a freeze-drying process (Figure 2).

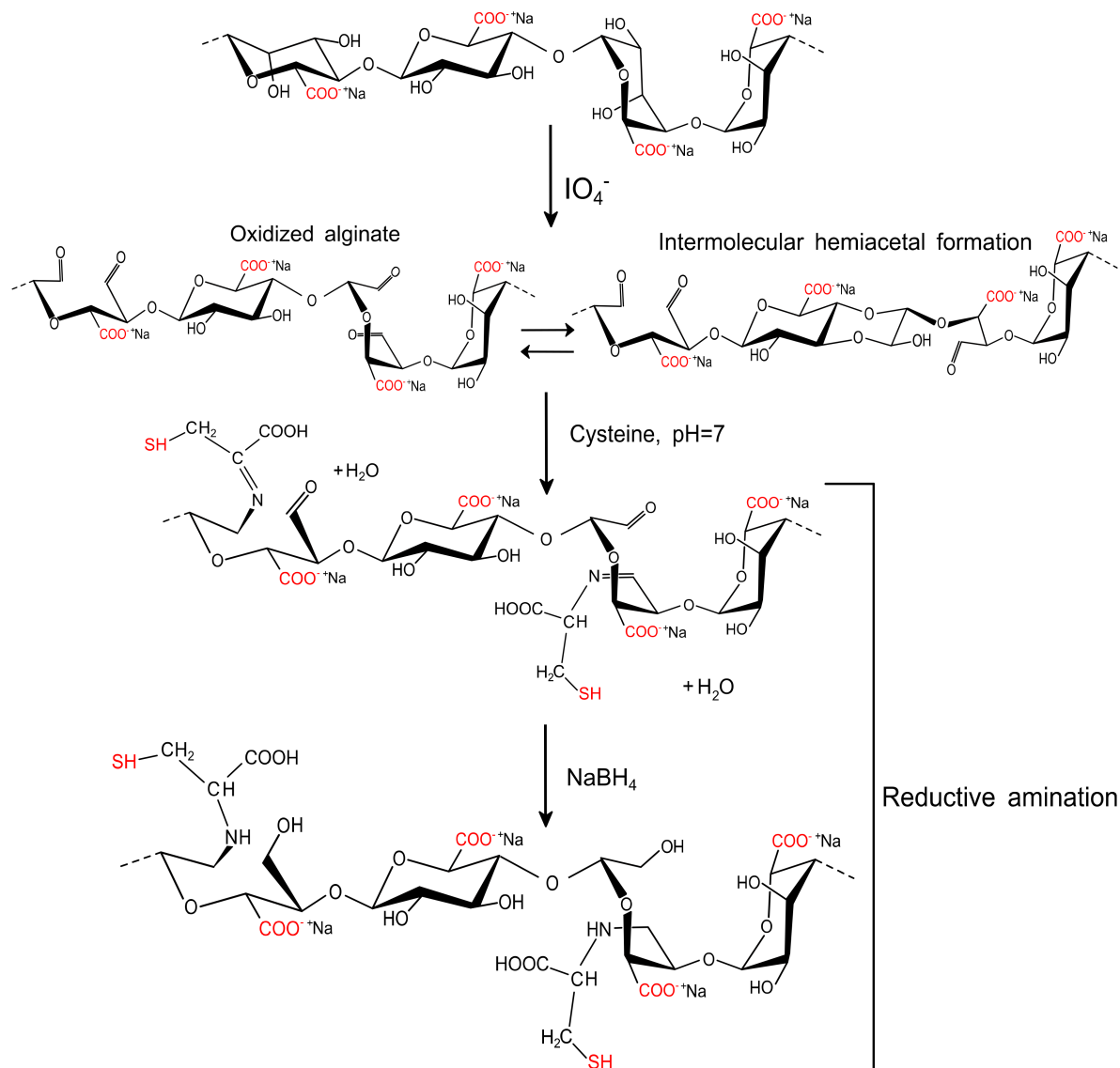


**Figure 2.** Proposed reaction for the functionalization of sodium alginate with cysteine employed by oxidation and reductive amination.

### 3. Characterization

#### 3.1. Evaluation of Polyphenols by UV-Vis

For this analysis, both phases (organic and aqueous) were collected and analyzed by UV-Vis in the range of 500–200 nm. UV-Vis analyses were performed with a UV-1800 Shimadzu scanning spectrophotometer.

#### 3.2. Evaluation of Thiols by UV-Vis

The presence of thiol groups was quantified spectrophotometrically using Ellman's reagent (DTNB, 5,5-dithio-bis (2-nitrobenzoic acid)) [44]. Then, 40.2 mg of AlgPOS was dissolved in a stock solution of  $0.1 \text{ mmol L}^{-1}$  DTNB prepared in PBS buffer. The quantity of thiol groups was estimated from a standard curve of L-cysteine.

#### 3.3. FT-IR Measurements

Fourier-Transform Infrared (FT-IR) measurements were performed during each step of alginate functionalization (AlgP, AlgPO and AlgPOS) using a Shimadzu IR Prestige-21 spectrometer with Attenuated Total Reflection (ATR). The spectra were acquired (64 scans/sample) in the range of  $4000\text{--}600 \text{ cm}^{-1}$  at room temperature with a resolution of  $4 \text{ cm}^{-1}$ . Deriva-

tions, including a Savitzky–Golay algorithm with 23 smoothing points, were analyzed with OriginLab 9.0 software.

### 3.4. $^1\text{H}$ NMR and HSQC Analyses of AlgP

In order to reach a degree of polymerization around 10–30, AlgP was hydrolyzed according to the procedure reported in the literature [45]. Then, 10 mg of hydrolyzed AlgP was dissolved in 500  $\mu\text{L}$  of  $\text{D}_2\text{O}$ . Next, TMSP- $\text{d}_4$ -3-(Trimethylsilyl)-propionic-2,2,3,3- $\text{d}_4$  acid sodium salt was added as an internal standard for the chemical shift. The  $^1\text{H}$  NMR spectrum was recorded on a Bruker Avance III-400 spectrometer at 80  $^\circ\text{C}$  and processed with TopSpin 3.2 software (Bruker BioSpin, Billerica, MA, USA).

### 3.5. Analysis of Alginate Derivatives by Solid State $^{13}\text{C}$ NMR

The analyses by solid state  $^{13}\text{C}$  NMR were performed in a Bruker Avance III-400 operating at 9.4 T magnetic field,  $\nu(^1\text{H}) = 400$  MHz. The  $^{13}\text{C}$  resonance frequency was 100.57 MHz with a pulse sequence (cross-polarization on magic-angle spinning (CP-MAS)) and CP-MAS with total sideband suppression (CP-MAS-TOSS). A high-power decoupling field was set at 83.3 kHz [ $P_{90}(^1\text{H}) = 3$   $\mu\text{s}$ ], and adamantane (38.5 ppm for  $\text{CH}_2$  resonance) was used as an external reference for adjustment of the  $^{13}\text{C}$  chemical shift.

## 4. Results and Discussion

### 4.1. Analysis of the Starting Material

Purification of commercial-grade alginates ought to be carried out prior to alginate functionalization, since production of this polysaccharide is based exclusively on extraction from brown seaweeds [46]. In this regard, short aliphatic chains like tert-butanol have been employed in the three-phase partitioning method for the bioseparation of proteins [47]. In contrast, n-butanol can be used for separating low-molecular substances present in alginates, including aromatic acids, hydroxyl acids, carbohydrates and polyols [48]. Hence, in this study, n-butanol was used, aiming to remove a significant quantity of substances commonly found in commercial-grade alginates. In Figure 3A, at around 280 nm, a signal can be seen probably by  $\pi$ – $\pi^*$  transitions attributed to the ring benzene present in polyphenols [6,49]. This asseveration is evidenced in the spectrum by its first derivative. Moreover, in Figure 3B, the organic phase shows its capability of extracting low-molecular-weight molecules and polyphenols owing to the presence of bands around 207 nm and 280 nm, attributed to the ring benzene present in phlorotannins [50,51]. Consequently, these bands could be assigned to polyphenols or similar molecules characterized by having a ring benzene, which may still remain in alginates.

Figure 4 shows the  $^1\text{H}$  NMR spectrum of AlgP for evaluating the M/G ratio according to the method described by S. Pawar and K. Edgar [52]. This parameter was calculated from the signals in the anomeric region (4.4–5.5 ppm) through the relationship of G and M block distribution [53,54]. In this case, the M/G value of commercial sodium alginate after the purification process with n-butanol is 1.02 (Table S2). This parameter directly influences the capacity to form gels through crosslinking reactions with divalent ions, since it is a well-known fact that alginates with a low M/G ratio produce stronger structures due to the high affinity of G blocks towards calcium ions. On the contrary, alginates with a high M/G ratio possess promising elastic properties and are able to form acidic gels [55,56]. Considering that AlgP is composed of almost 50% of each uronic acid, oxidation and reductive amination processes could be studied to evaluate the susceptibility of hemiacetal formation in G or M blocks, as well as their effect on cysteine after the reductive amination process. The application of solid state NMR spectroscopy for analyzing the linking of nitrogen-containing molecules and the presence of thiol groups have been reported elsewhere [57]. For this reason,  $^{13}\text{C}$  CP-MAS NMR spectra of alginate derivatives were studied in detail and discussed in terms of the results obtained by second derivative FT-IR analysis.

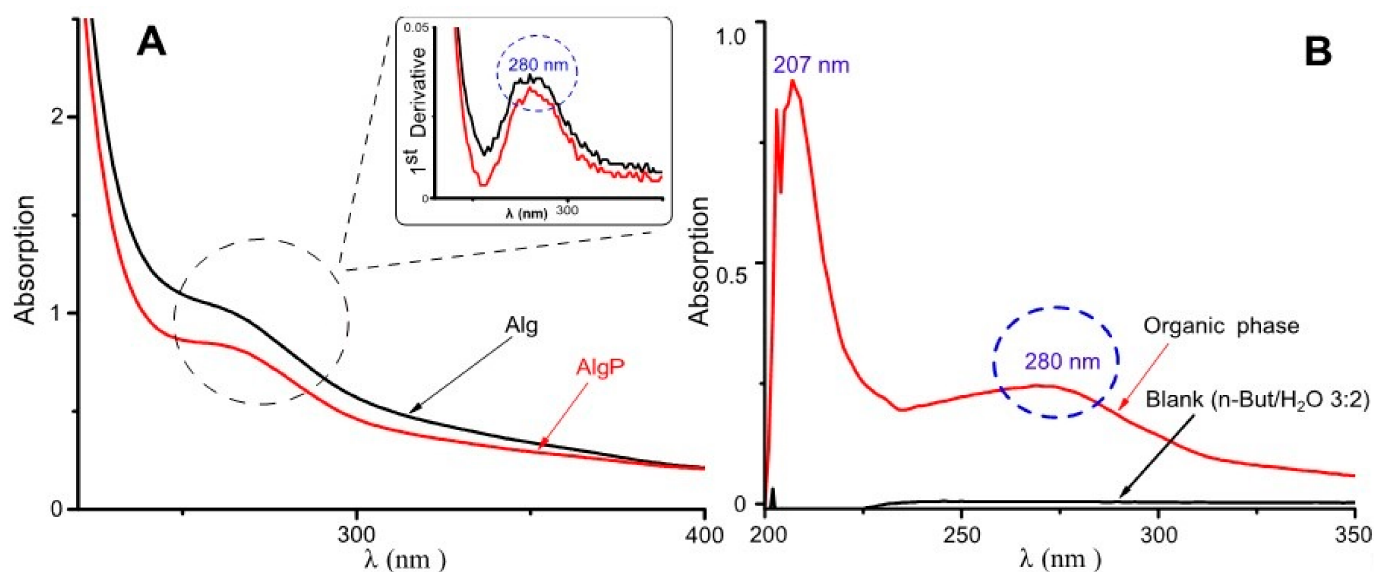


Figure 3. UV-Visible spectra for alginate purification. (A) Aqueous phase with the first derivative. (B) Organic phase.

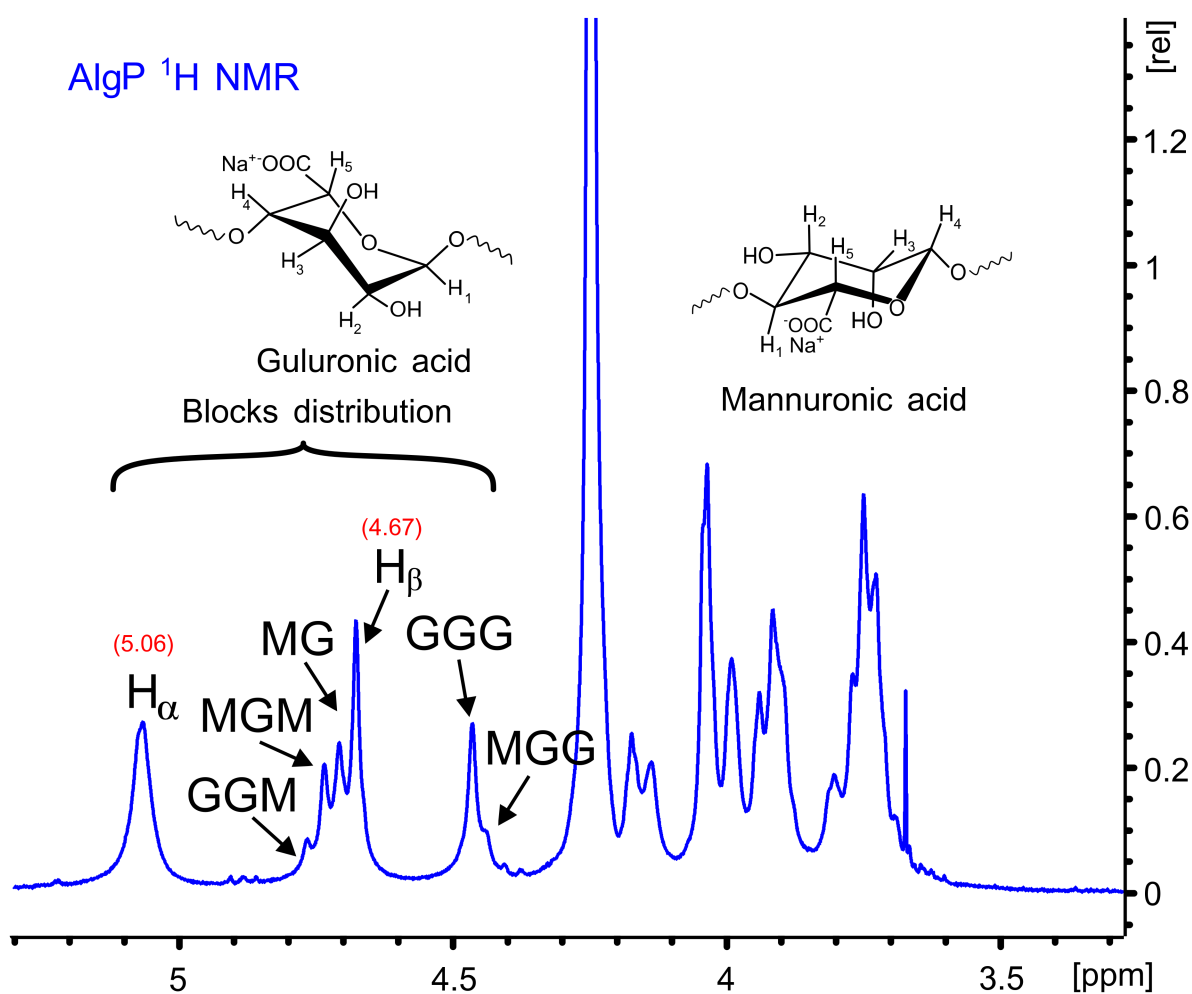


Figure 4. <sup>1</sup>H NMR spectrum of AlgP.

The <sup>1</sup>H and <sup>13</sup>C NMR chemical shifts of AlgP are depicted in Table 1. For a better interpretation of AlgP's structure, Figure 5 displays the <sup>13</sup>C/<sup>1</sup>H HSQC spectrum of AlgP

in order to evaluate the correlation between  $^{13}\text{C}$ - $^1\text{H}$  (Table 1). As can be observed, the 103.92/4.67 ppm correlation was assigned to  $\text{C}_1/\text{H}_1$  of  $\beta$ -D-mannuronic acid residues, whereas the signal at 102.70/5.06 ppm was attributed to  $\text{C}_1/\text{H}_1$  of  $\alpha$ -L-guluronic acid residue. The 80.78/3.91 ppm and 82.63/4.13 ppm correlations were assigned to  $\text{C}_4/\text{H}_4$  of manuronic ( $\text{AlgP}^a$ ) and guluronic ( $\text{AlgP}^b$ ) acid residues in AlgP.

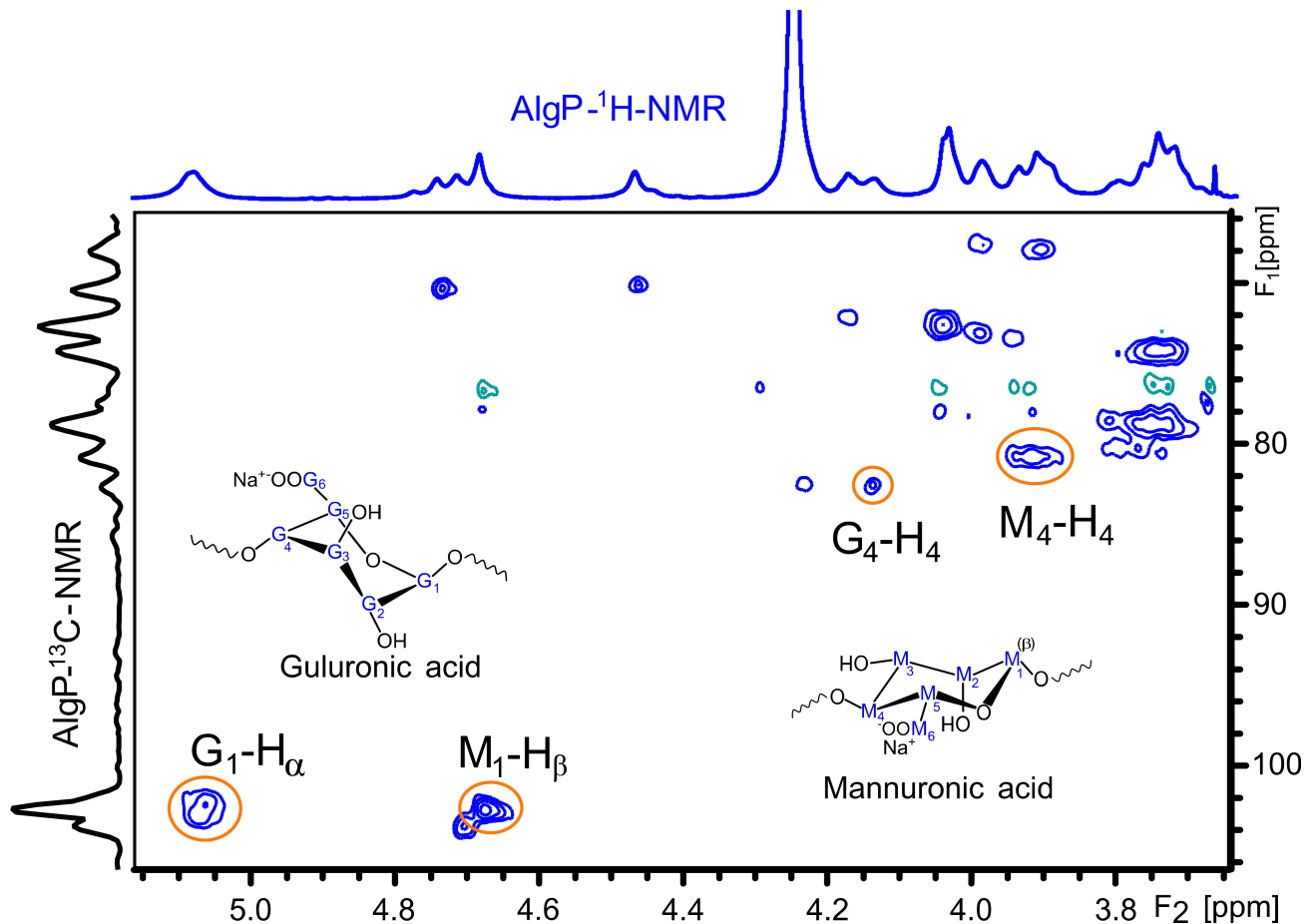


Figure 5. HSQC spectrum of purified alginate (AlgP).

Table 1. Assignment of the chemical shifts of AlgP  $^1\text{H}$  NMR.

Sample	$\delta$ (ppm)										
	H-1	C-1	H-2	C-2	H-3	C-3	H-4	C-4	H-5	C-5	C-6
AlgP <sup>a</sup>	4.67	103.92	4.02	72.58	3.74	74.11	3.91	80.78	3.75	78.79	175.4
AlgP <sup>b</sup>	5.06	102.67	3.98	67.78	4.17	72.23	4.13	82.63	4.46	70.14	176.1

<sup>a</sup> Chemical shifts for mannuronic acid residue in AlgP. <sup>b</sup> Chemical shifts for guluronic acid residue in AlgP.

## 4.2. Evaluation of Alginate Functionalization

### 4.2.1. FT-IR spectroscopy

Figure 6 depicts three different ATR-IR spectra obtained during each step of alginate functionalization. The typical signals around  $1598\text{ cm}^{-1}$  and  $1411\text{ cm}^{-1}$  were assigned to asymmetric and symmetric movements of carboxylate groups present in the structure despite the functionalization process. According to this, carboxylate groups are not affected considerably by oxidation and reductive amination processes. In contrast, the band associated with C-O stretching vibration of pyranose rings was clearly affected, as is demonstrated with the chemical shifts from  $1024\text{ cm}^{-1}$  to  $1014\text{ cm}^{-1}$  (after periodate

oxidation), and then to  $1020\text{ cm}^{-1}$  due to the structural modification with cysteine. The bands at  $1122\text{ cm}^{-1}$  and  $1083\text{ cm}^{-1}$  assigned to C-O and C-C stretching vibrations of pyranose rings [58] were also affected by structural changes produced by functionalization with cysteine.

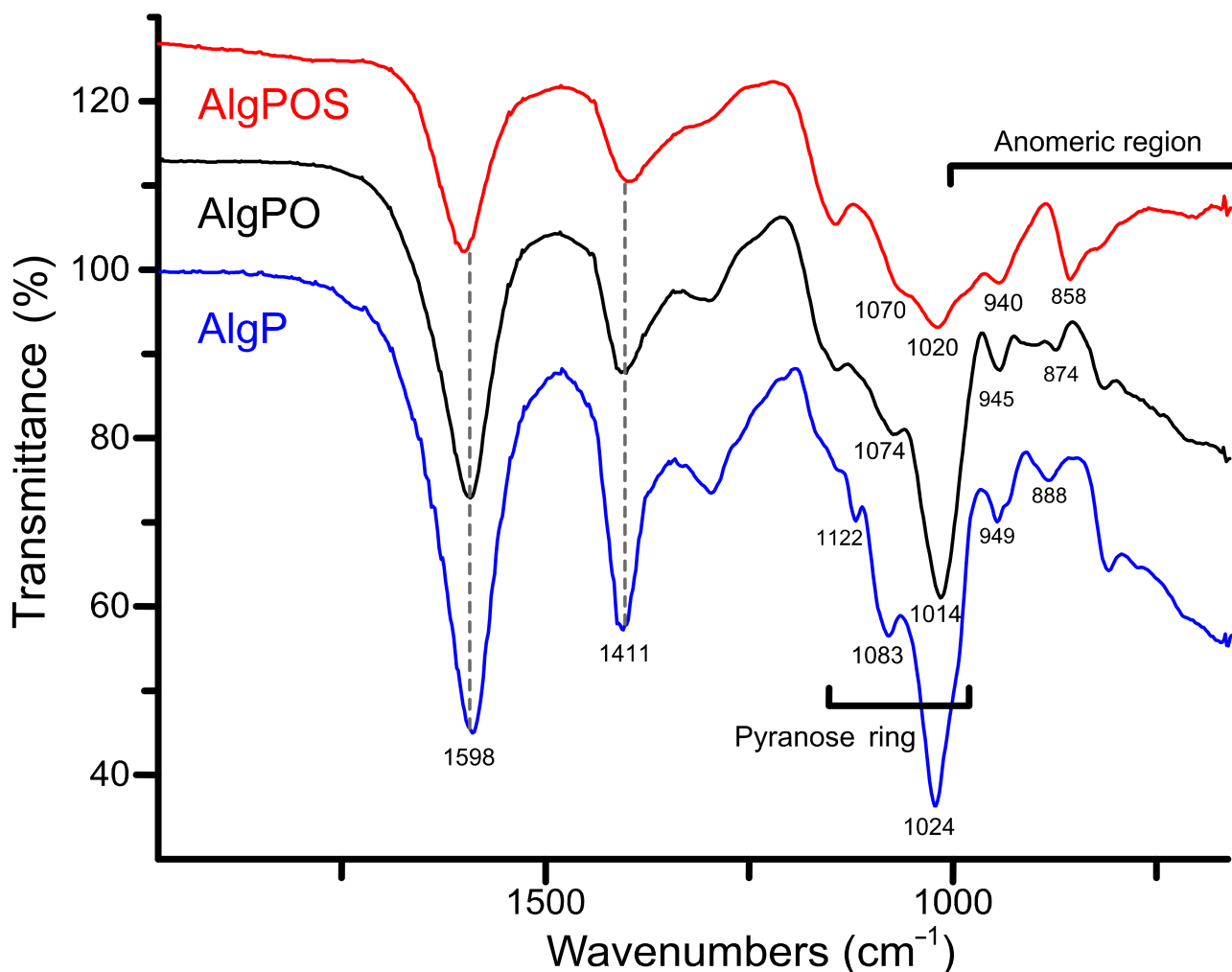


**Figure 6.** ATR-IR spectra of the starting material (AlgP), oxidized alginate (AlgPO) and alginate-based material (AlgPOS).

With regard to the anomeric region around  $1000\text{--}750\text{ cm}^{-1}$ , the spectra exhibit a band at  $949\text{ cm}^{-1}$  assigned to C-O stretching vibration of uronic acid residues, while the band at  $888\text{ cm}^{-1}$  is assigned to  $C_1\text{-H}$  deformation vibration of  $\beta$ -D mannuronic acid residues [59].

In order to improve the resolution of overlapping bands in the normal FT-IR spectrum [60], the second-derivative FT-IR technique was applied for analyzing alginate derivatives—as this method has been widely used for structural analysis of macromolecules [32,59,61]. Thus, in Figure 6, the C-O and C-C stretching vibrations were found at  $1122\text{ cm}^{-1}$  for AlgP. This band was considerably affected by oxidation, as well as the reductive amination process, and, therefore, this band vanished in AlgPO and AlgPOS spectra. Another similar situation is observed in Figure 7 since the band at  $1170\text{ cm}^{-1}$  (second derivative) is assigned to the C-O stretching vibration of the glycosidic linkage of AlgP; this band was affected in each step of the functionalization, resulting in a chemical shift towards  $1161\text{ cm}^{-1}$  for AlgPO (second derivative), whereas this band was at  $1150\text{ cm}^{-1}$  for AlgPOS (second derivative). The C-O and C-C stretching vibrations of pyranose rings (observed at  $1083\text{ cm}^{-1}$ ) were shifted to  $1074\text{ cm}^{-1}$  (second derivative) and  $1070\text{ cm}^{-1}$  (second derivative) because of oxidation and the reductive amination process, respectively. These bands are possibly shifting due to the Malaprade reaction, as periodates do indeed cleave the pyranose ring



between C<sub>2</sub> and C<sub>3</sub>. This procedure is the best route to oxidize diols into aldehydes under dark conditions (Figure 3). Additionally, the reductive amination process using cysteine leads to the formation of imines, which are reduced with sodium borohydride (Figure 3). It must be noted that the second-derivative technique is very useful for studying the anomeric region, where bands at 949 cm<sup>-1</sup> (AlgP), 945 cm<sup>-1</sup> (AlgPO) and 940 cm<sup>-1</sup> (AlgPOS, second derivative), associated with C-O stretching vibration, shifted to lower vibration frequencies as a consequence of the new environment caused by the ring opening and post introduction of cysteine molecules into the polymer chain.

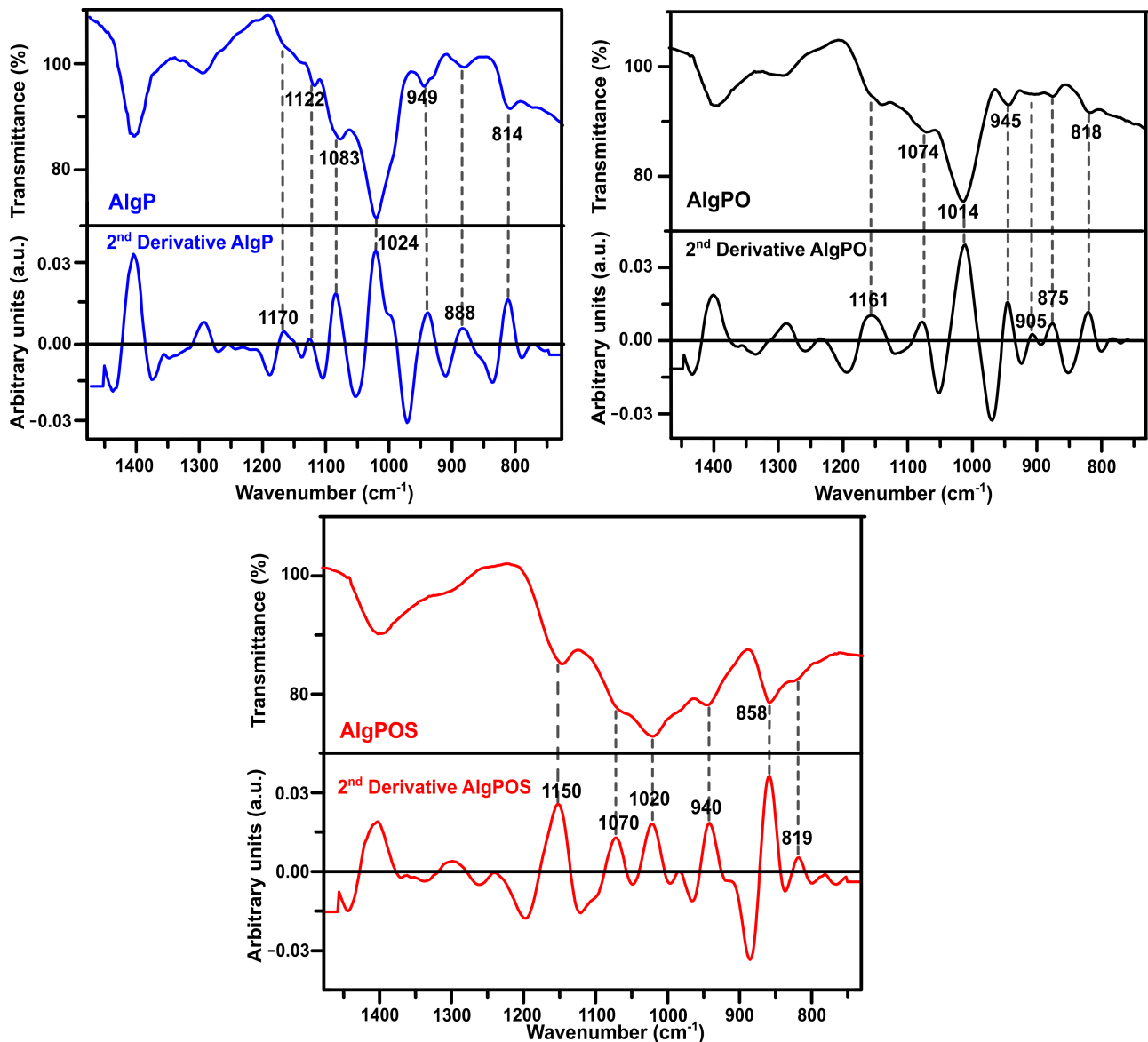


**Figure 7.** Second-derivative ATR-IR spectra of the starting material (AlgP), oxidized alginate (AlgPO) and alginate-based material (AlgPOS).

According to Matsuhiro et al. [62], the alginate always exhibits two characteristic bands associated with the C<sub>1</sub>-H anomeric of  $\beta$ -D-mannuronic acid at around 888 cm<sup>-1</sup>, and another band at 902 cm<sup>-1</sup> characteristic of C<sub>1</sub>-H of  $\alpha$ -L-guluronic acid residue. In AlgPO and AlgPOS, it could be observed how these signals were affected due to the degradation process of blockchains caused by the functionalization process (Figure 7) [63]. Furthermore, the band at around 814 cm<sup>-1</sup> is assigned to COH, CCH and OCH stretching vibrations of  $\alpha$ -L-guluronic acid residues, with a contribution of bending deformation

vibrations of C-O-C glycosidic linkages in homopolymeric blocks [58,59]. This band is clearly observed at  $818\text{ cm}^{-1}$  in the normal ATR-IR spectrum of AlgPO. However, without the utilization of the second-derivative technique, it would be challenging to detect the signal at  $819\text{ cm}^{-1}$ , which was overlapped in the classical ATR-IR spectrum of AlgPOS. Finally, the band observed at  $858\text{ cm}^{-1}$  may be assigned to N-H stretching vibration as a consequence of cysteine molecules [64]. The presence of thiol groups in the alginate structure was corroborated through the Ellman method (Figure S2), reporting  $185\text{ }\mu\text{mol}$  thiol groups per gram of AlgPOS, as shown in Table S3.

#### 4.2.2. Analysis of Alginate and Its Derivatives by $^{13}\text{C}$ NMR in Solid State

The effect ascribed to the chemical reactions during alginate functionalization was studied by the FT-IR technique and confirmed by using  $^{13}\text{C}$  NMR in solid state. Figure 8 displays the spectrum of AlgP, and its characteristic peaks are assigned in Table 2. Owing to the oxidation produced by the utilization of sodium metaperiodate as an oxidizing agent, a new peak emerges at  $92.8\text{ ppm}$  attributed to hemiacetal groups formed by intramolecular interactions between aldehyde groups of oxidized residues and hydroxyl groups of unoxidized hydroxyl moieties that were situated in neighboring positions of the same polymer chain [65]. To achieve an effective functionalization via reductive amination, crucial factors must be controlled to form the imine bond successfully, e.g., pH, reaction time and the amount of nitrogen-containing molecules [32]. As we demonstrated in a previous work, thiosemicarbazide ( $\text{NH}_2\text{-NH-(C=S)-NH}_2$ ) promotes crosslinking reactions between both terminal primary amine groups present in the molecule and oxidized moieties of alginate [66]. Thus, a strict control of  $\text{pH} \approx 7$  and reaction time above 24 h can guarantee the formation of imine bonds between cysteine molecules and hemiacetal groups, which revert back to aldehyde form in aqueous medium during the reductive amination process [32]. In addition, a high concentration of buffer makes it feasible to avoid the formation of thiazolidine, a side product that is produced by the interaction between thiols and aldehydes [67]. In these conditions, this side reaction would not be favorable on thermodynamic grounds [32,67]. On the other hand, it has been previously reported that the  $-\text{CH}_2\text{-SH}$  moiety appears at  $28.8\text{ ppm}$  [57]. Thus, we have considered that the peak at  $31.2\text{ ppm}$  is attributed to  $-\text{CH}_2\text{-SH}$  of the cysteine attached to the alginate backbone. This new peak is present in the spectra due to the efficient reductive amination process, performed in order to achieve the functionalization of alginate. The resonances of both the M-6 and G-6 contribution at  $176.2\text{ ppm}$  assigned to carboxylate groups have not been altered, which is clear evidence that sodium metaperiodate is a suitable oxidizing agent to convert diols into aldehydes without affecting carboxylate groups. The pyranose region showed considerable structure changes associated with guluronic residue. The signals corresponding to G-4 grew smaller along each step of the functionalization process. Several signals obtained by NMR in solid state consisted of contributions from more carbon sites within each mannuronic and guluronic acid residue, due to chemical shift distribution [53]. Thus, the signal of  $68.8\text{ ppm}$  in AlgP contains a contribution of G-3 and G-5, which is noticeably affected by periodate oxidation in AlgPO and AlgPOS (Table 2). Additionally, the intensity of the peaks at  $102.6\text{ ppm}$  (G-1) and  $99.6\text{ ppm}$  (M-1), associated with the  $\text{C}_1\text{-H}$  anomeric of  $\alpha\text{-L-guluronic acid}$  residue and  $\text{C}_1\text{-H}$  of  $\beta\text{-D-mannuronic acid}$ , respectively [53], have both shown a decrease due to rupture of glycosidic linkage, due to severely affected carbon atoms associated with  $\alpha\text{-L-guluronic acid}$  residues as displayed in Figure 8.

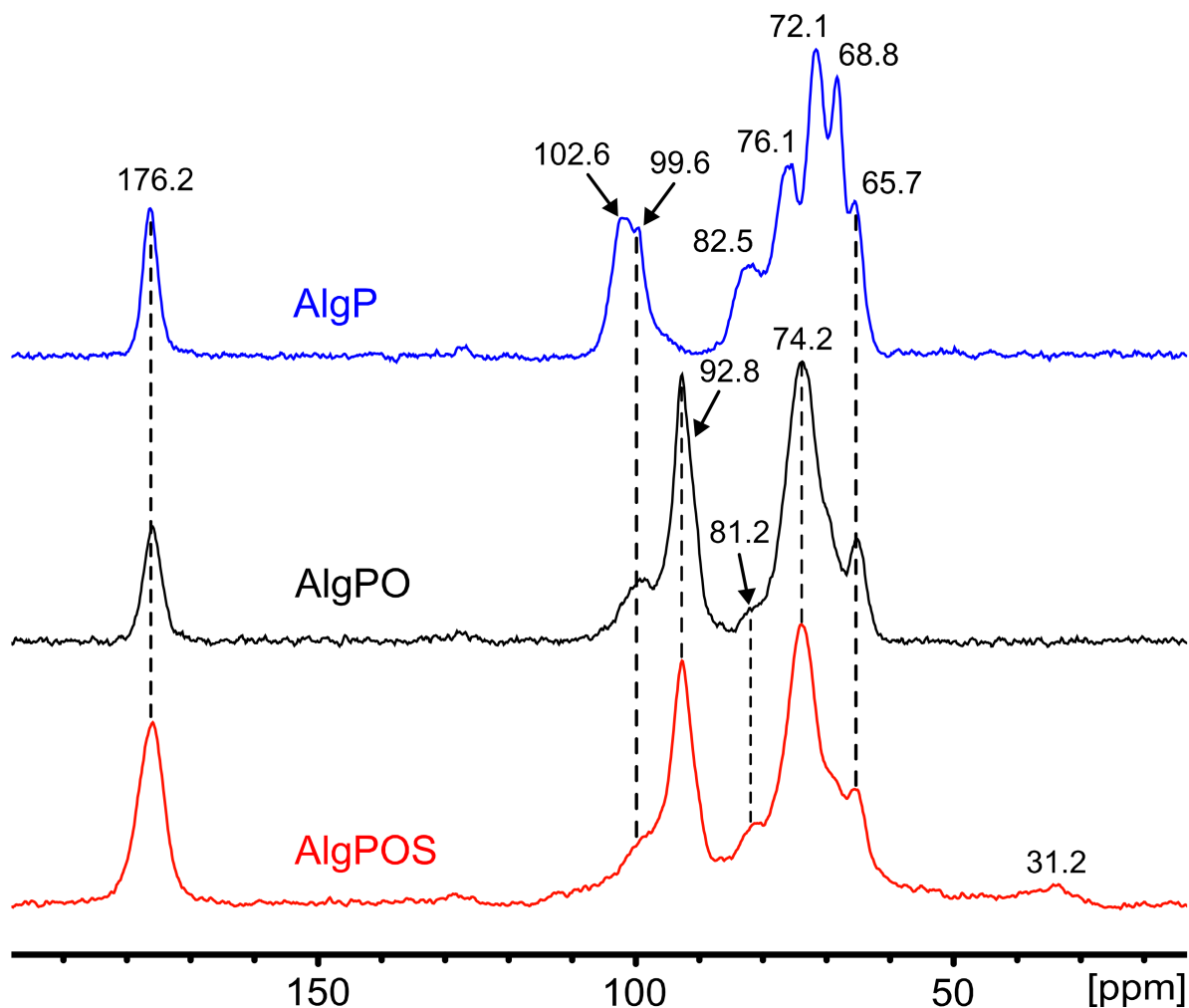


**Figure 8.**  $^{13}\text{C}$  NMR in solid state in each step of functionalization. i. Starting material (AlgP), ii. Oxidized alginate (AlgPO) and iii. Alginate after reductive amination (AlgPOS).

Conversely, the signals corresponding to M have not shown a significant change, as the peaks at 74.2 ppm could be a contribution of both signals at 72.1 ppm and 76.1 ppm, assigned to M-2 and M-4, respectively. These results suggest that G units of AlgPO are preferentially oxidized since G units were greatly affected rather than M—in spite of being present in the alginate structure in almost equal proportions (M/G ratio 1.02). Nevertheless, other factors like block distribution might be more important than the M/G ratio, especially when the M/G ratio gives an almost equal proportion of M and G blocks, as is reported in this work. Since G residue is more reactive than M to cleavage, the stability of these oxidized groups will depend on their neighbors. These might stabilize them, forming hemiacetal groups, or might be affected by a fast hydrolyzation, which would lead to a decrease in alginate-based material formation [68,69]. To conclude, the effect of the reducing agent during the reductive amination process depends on several factors [70] and, thus, the utilization of a specific borohydride derivative ought to be explored, taking into account that sodium cyanoborohydride generates the presence of HCN, NaCN and cyanoborohydride derivatives that are highly toxic for the environment and human beings [71,72]. Hence, according to the literature, sodium borohydride is a low-cost and efficient reagent that can be used during the reductive amination process under different conditions with good yields [73,74].

**Table 2.** Assignment of the chemical shifts by  $^{13}\text{C}$  NMR in solid state.

Assignment of M (mannuronic) or G (guluronic) carbons	$\delta$ (ppm)												
	Anomeric				Pyranose				Carboxylate		Hemiacetal	$-\text{CH}_2\text{-SH}$	
	G-1	M-1	G-4	M-5	M-4	M-2	M-3	G-3	G-5	G-2	M-6	G-6	
AlgP	102.6	99.6	82.5	76.1		72.1		68.8		65.7	176.2	-	-
AlgPO	-	99.6	81.2			74.2		-		65.7	176.2	92.8	-
AlgPOS	-	99.6	81.2			74.2		-		65.7	176.2	92.8	31.2

## 5. Conclusions

In summation, the functionalization of purified sodium alginate was achieved successfully via oxidation and the reductive amination process. In order to evaluate the chemical modification using a purified raw material (AlgP), polyphenols and phlorotannins were removed from commercial-grade alginate using n-butanol. Characterization of AlgP shows a M/G of 1.02, whereas HSQC studied correlations of  $^1\text{H}$ - $^{13}\text{C}$ . AlgPOS demonstrated cysteine covalently bound to the alginate with a coupling around 185  $\mu\text{mol}$  of attached thiol groups per gram of polymer as estimated by UV-Vis. FT-IR and solid state  $^{13}\text{C}$  NMR analyses confirmed the functionalization of alginate, as peaks were significantly displaced from their natural position. Around the pyranose and fingerprint regions, we observed two peaks at 99.2 ppm and 31.2 ppm, respectively. These peaks were attributed to hemiacetal formation due to the interaction of activated/deactivated aldehydes obtained by oxidation, whereas the attaching of cysteine to the alginate backbone caused an upfield resonance characteristic of  $\text{CH}_2\text{-SH}$  moieties from cysteine. The chemical shifts and vanished signals to G2 and G4 and G1, G3 and G5, respectively, in AlgPOS by  $^{13}\text{C}$  NMR demonstrated the susceptibility of guluronic groups in the process of functionalization.

**Supplementary Materials:** The following are available online at <https://www.mdpi.com/2073-4360/13/2/255/s1>, Figure S1: Refractive index chromatogram of commercial sodium alginate used as starting material., Figure S2. UV-Vis spectra of cysteine standards (E1, E2 and E3) and AlgPOS. Evaluation of the thiol group by Ellman's reaction. Table S1. Values obtained of commercial sodium alginate by SEC-MALS., Table S2. Values obtained of commercial sodium alginate by  $^1\text{H}$  NMR., Table S3. Values obtained of AlgPOS by UV-Vis.

**Author Contributions:** Investigation and formal analysis, R.G.H.-P.; writing—original draft preparation, R.G.H.-P. and E.R.P.L.; writing—review and editing, R.G.H.-P., A.C.V., B.M.C. and T.V.; conceptualization and supervision, R.G.H.-P., A.C.V. and T.V.; funding acquisition, A.C.V. All authors have read and agreed to the published version of the manuscript.

**Funding:** This research was funded by the Ministry of Education (MINEDU) of Peru through the inter institutional cooperation agreement between MINEDU (N $^{\circ}$  401-2017-MINEDU) and The National University of Engineering (UNI) as well as the Master of Science Program (N $^{\circ}$  208-2015-FONDECYT).

**Institutional Review Board Statement:** Not applicable.

**Informed Consent Statement:** Not applicable.

**Data Availability Statement:** The data presented in this study are available on request from the corresponding author.

**Acknowledgments:** The authors Ronny G. Huamani and Bryan M. Córdova are thankful to “Escuela Central de Posgrado de la Universidad Nacional de Ingeniería” as well as “Rectorado” UNI for supporting the research stay in NTNU-Norway. The authors also thank Olav Aarstad for kindly providing the SEC-MALS analysis of the starting material.

**Conflicts of Interest:** The authors declare no conflict of interest.

## References

- Hernandez-Carmona, G.; Mchugh, D.J.; Arvizu-higuera, D.L.; Rodriguez, E. Pilot plant scale extraction of alginate from *Macrocystis pyrifera*. 1. Effect of pre-extraction treatments on yield and quality of alginate. *Environ. Boil. Fishes* **1999**, *10*, 507–513.

2. Acleto, C. The seaweed resources of Peru. In *Seaweed Resources of the World*; Critchley, A.T., Ohno, M., Eds.; Japan International Cooperation Agency: Tokyo, Japan, 1998; p. 431.
3. Tiwari, B.K.; Troy, D.J. *Seaweed Sustainability: Food and Non-Food Applications*; Academic Press: Cambridge, MA, USA, 2015; ISBN 9780124199583.
4. Hernández-Carmona, G.; Freile-Pelegrín, Y.; Hernández-Garibay, E. *Conventional and Alternative Technologies for the Extraction of Algal Polysaccharides*; Woodhead Publishing: Sawston, UK, 2013; pp. 475–516. ISBN 9780857095121.
5. Indergaard, M.; Skjåk-Bræk, G. Characteristics of alginate from *Laminaria digitata* cultivated in a high-phosphate environment. *Hydrobiologia* **1987**, *151–152*, 541–549. [[CrossRef](#)]
6. Wijesekara, I.; Kim, S.K.; Li, Y. Phlorotannins as bioactive agents from brown algae. *Process Biochem.* **2011**, *46*, 2219–2224. [[CrossRef](#)]
7. Matsuhiro, B. Characterization of a fucoidan from *Lessonia vadosa* (Phaeophyta) and its anticoagulant and elicitor properties. *Int. J. Biol. Macromol.* **2008**, *42*, 235–240.
8. Lee, K.Y.; Mooney, D.J. Alginate: Properties and biomedical applications. *Prog. Polym. Sci.* **2012**, *37*, 106–126. [[CrossRef](#)] [[PubMed](#)]
9. Draget, K.I.; Taylor, C. Chemical, physical and biological properties of alginates and their biomedical implications. *Food Hydrocoll.* **2011**, *25*, 251–256. [[CrossRef](#)]
10. Mazumder, A.; Holdt, S.L.; De Francisci, D.; Alvarado-Morales, M.; Mishra, H.N.; Angelidaki, I. Extraction of alginate from *Sargassum muticum*: Process optimization and study of its functional activities. *J. Appl. Phycol.* **2016**, *28*, 3625–3634. [[CrossRef](#)]
11. Rhein-Knudsen, N.; Ale, M.T.; Ajallouei, F.; Meyer, A.S. Characterization of alginates from Ghanaian brown seaweeds: *Sargassum* spp. and *Padina* spp. *Food Hydrocoll.* **2017**, *71*, 236–244. [[CrossRef](#)]
12. Valeur, M.; Markussen, S.; Ellingsen, T.E.; Skjåk-bræk, G. Influence of environmental conditions on the activity of the recombinant mannuronan C-5-epimerase AlgE2. *Enzym. Microb. Technol.* **2001**, *28*, 57–69.
13. Tøndervik, A.; Klinkenberg, G.; Aachmann, F.L.; Svanem, B.I.G.; Ertesvåg, H.; Ellingsen, T.E.; Valla, S.; Skjåk-bræk, G.; Sletta, H. Mannuronan C-5 epimerases suited for tailoring of specific alginate structures obtained by high-throughput screening of an epimerase mutant library. *Biomacromolecules* **2013**, *14*, 2657–2666. [[CrossRef](#)]
14. Ilmi, Z.N.; Wulandari, P.A.C.; Husen, S.A.; Winarni, D.; Alamsjah, M.A.; Awang, K.; Vastano, M.; Pellis, A.; Macquarrie, D.; Pudjiastuti, P. Characterization of alginate from *sargassum duplicatum* and the antioxidant effect of alginate-okra fruit extracts combination for wound healing on diabetic mice. *Appl. Sci.* **2020**, *10*, 6082. [[CrossRef](#)]
15. Keil, C.; Hübner, C.; Richter, C.; Lier, S.; Barthel, L.; Meyer, V.; Subrahmanyam, R.; Gurikov, P.; Smirnova, I.; Haase, H. Ca-Zn-Ag Alginate Aerogels for Wound Healing Applications: Swelling Behavior in Simulated Human Body Fluids and Effect on Macrophages. *Polymers* **2020**, *12*, 2741. [[CrossRef](#)] [[PubMed](#)]
16. Patwa, R.; Zandrea, O.; Capáková, Z.; Saha, N.; Saha, P. Effect of iron-oxide nanoparticles impregnated bacterial cellulose on overall properties of alginate/casein hydrogels: Potential injectable biomaterial for wound healing applications. *Polymers* **2020**, *12*, 2690. [[CrossRef](#)] [[PubMed](#)]
17. Bevilacqua, A.; Campaniello, D.; Speranza, B.; Racioppo, A.; Altieri, C.; Sinigaglia, M.; Corbo, M.R. Microencapsulation of *saccharomyces cerevisiae* into alginate beads: A focus on functional properties of released cells. *Foods* **2020**, *9*, 1051. [[CrossRef](#)] [[PubMed](#)]
18. Valente, J.F.A.; Dias, J.R.; Sousa, A.; Alves, N. Composite central face design-an approach to achieve efficient alginate microcarriers. *Polymers* **2019**, *11*, 1949. [[CrossRef](#)] [[PubMed](#)]
19. Kühn, P.T.; Rozenbaum, R.T.; Perrels, E.; Sharma, P.K.; van Rijn, P. Anti-microbial biopolymer hydrogel scaffolds for stem cell encapsulation. *Polymers* **2017**, *9*, 149. [[CrossRef](#)]
20. Huang, C.H.; Chuang, T.J.; Ke, C.J.; Yao, C.H. Doxorubicin-gelatin/Fe<sub>3</sub>O<sub>4</sub>-Alginate dual-layer magnetic nanoparticles as targeted anticancer drug delivery vehicles. *Polymers* **2020**, *12*, 1747. [[CrossRef](#)]
21. Cheaburu-Yilmaz, C.N.; Lupuşoru, C.E.; Vasile, C. New alginate/PNIPAAm matrices for drug delivery. *Polymers* **2019**, *11*, 366. [[CrossRef](#)]
22. Alnaief, M.; Obaidat, R.M.; Alsmadi, M.M. Preparation of hybrid alginate-chitosan aerogel as potential carriers for pulmonary drug delivery. *Polymers* **2020**, *12*, 2223. [[CrossRef](#)]
23. Bernkop-Schnürch, A.; Greimel, A. Thiomers: The next generation of mucoadhesive polymers. *Am. J. Drug Deliv.* **2005**, *3*, 141–154. [[CrossRef](#)]
24. Draget, K.I.; Skjåk-Braek, G. Alginates: Existing and potential biotechnological and medical applications. *RSC Polym. Chem. Ser.* **2011**, *1*, 186–209.
25. Szabó, L.; Gerber-Lemaire, S.; Wandrey, C. Strategies to Functionalize the Anionic Biopolymer Na-Alginate without Restricting Its Polyelectrolyte Properties. *Polymers* **2020**, *12*, 919. [[CrossRef](#)]
26. Martí, M.; Frigols, B.; Salesa, B.; Serrano-Aroca, Á. Calcium alginate/graphene oxide films: Reinforced composites able to prevent *Staphylococcus aureus* and methicillin-resistant *Staphylococcus epidermidis* infections with no cytotoxicity for human keratinocyte HaCaT cells. *Eur. Polym. J.* **2019**, *110*, 14–21. [[CrossRef](#)]
27. Salesa, B.; Martí, M.; Frigols, B.; Serrano-Aroca, Á. Carbon nanofibers in pure form and in calcium alginate composites films: New cost-effective antibacterial biomaterials against the life-threatening multidrug-resistant *Staphylococcus epidermidis*. *Polymers* **2019**, *11*, 453. [[CrossRef](#)]

28. Ma, X.; Li, R.; Zhao, X.; Ji, Q.; Xing, Y.; Sunarso, J.; Xia, Y. Biopolymer composite fibres composed of calcium alginate reinforced with nanocrystalline cellulose. *Compos. Part A Appl. Sci. Manuf.* **2017**, *96*, 155–163. [[CrossRef](#)]
29. Córdova, B.M.; Venâncio, T.; Olivera, M.; Huamani-Palomino, R.G.; Valderrama, A.C. Xanthation of alginate for heavy metal ions removal. Characterization of xanthate-modified alginates and its metal derivatives. *Int. J. Biol. Macromol.* **2021**, *169*, 130–142. [[CrossRef](#)]
30. Albrecht, K.; Bernkop-Schnürch, A. Thiomers: Forms, functions and applications to nanomedicine. *Nanomedicine* **2007**, *2*, 41–50. [[CrossRef](#)]
31. Bernkop-Schnürch, A. Thiomers: A new generation of mucoadhesive polymers. *Adv. Drug Deliv. Rev.* **2005**, *57*, 1569–1582. [[CrossRef](#)]
32. Huamani-Palomino, R.G.; Jacinto, C.R.; Alarcón, H.; Mejía, I.M.; López, R.C.; de Silva, D.O.; Cavalheiro, E.T.G.; Venâncio, T.; Dávalos, J.Z.; Valderrama, A.C. Chemical modification of alginate with cysteine and its application for the removal of Pb(II) from aqueous solutions. *Int. J. Biol. Macromol.* **2019**, *129*, 1056–1068. [[CrossRef](#)]
33. Grewal, P.; Mundlia, J.; Ahuja, M. Thiol modified Moringa gum—A potential bioadhesive polymer. *Carbohydr. Polym.* **2019**, *209*, 400–408. [[CrossRef](#)]
34. Puri, V.; Sharma, A.; Kumar, P.; Singh, I. Thiolation of biopolymers for developing drug delivery systems with enhanced mechanical and mucoadhesive properties: A review. *Polymers* **2020**, *12*, 1803. [[CrossRef](#)] [[PubMed](#)]
35. Hintzen, F.; Hauptstein, S.; Perera, G.; Bernkop-Schnürch, A. Synthesis and in vitro characterization of entirely S-protected thiolated pectin for drug delivery. *Eur. J. Pharm. Biopharm.* **2013**, *85*, 1266–1273. [[CrossRef](#)]
36. Kurniawan, D.W.; Fudholi, A.; Susidarti, R.A. Synthesis of Thiolated Chitosan as Matrix for the Preparation of Metformin Hydrochloride Microparticles. *Res. Pharm.* **2012**, *2*, 26–35.
37. Madison, S.A.; Carnali, J.O. PH optimization of amidation via carbodiimides. *Ind. Eng. Chem. Res.* **2013**, *52*, 13547–13555. [[CrossRef](#)]
38. Yang, Y. *Side Reactions in Peptide Synthesis*; Academic Press: Cambridge, MA, USA, 2015; Volume 43, pp. 1–326. ISBN 9780128011812.
39. Prokopijevic, M.; Prodanovic, O.; Spasojevic, D.; Kovacevic, G.; Polovic, N.; Radotic, K.; Prodanovic, R. Tyramine-modified pectins via periodate oxidation for soybean hull peroxidase induced hydrogel formation and immobilization. *Appl. Microbiol. Biotechnol.* **2017**, *101*, 2281–2290. [[CrossRef](#)] [[PubMed](#)]
40. Dalheim, M.; Vanacker, J.; Najmi, M.A.; Achmann, F.L.; Strand, B.L.; Christensen, B.E. Efficient functionalization of alginate biomaterials. *Biomaterials* **2016**, *80*, 146–156. [[CrossRef](#)]
41. Bouhadir, K.H.; Lee, K.Y.; Alsberg, E.; Damm, K.L.; Anderson, K.W.; Mooney, D.J. Degradation of partially oxidized alginate and its potential application for tissue engineering. *Biotechnol. Prog.* **2001**, *17*, 945–950. [[CrossRef](#)]
42. Christensen, B.E.; Vold, I.M.N.; Vårum, K.M. Chain stiffness and extension of chitosans and periodate oxidised chitosans studied by size-exclusion chromatography combined with light scattering and viscosity detectors. *Carbohydr. Polym.* **2008**, *74*, 559–565. [[CrossRef](#)]
43. Balakrishnan, B.; Lesieur, S.; Labarre, D.; Jayakrishnan, A. Periodate oxidation of sodium alginate in water and in ethanol-water mixture: A comparative study. *Carbohydr. Res.* **2005**, *340*, 1425–1429. [[CrossRef](#)]
44. Hauptstein, S.; Müller, C.; Dünnhaupt, S.; Laffleur, F.; Bernkop-Schnürch, A. Preactivated thiomers: Evaluation of gastroretentive minitables. *Int. J. Pharm.* **2013**, *456*, 473–479. [[CrossRef](#)]
45. Stanisci, A.; Aarstad, O.A.; Tøndervik, A.; Sletta, H.; Dypås, L.B.; Skjåk-Bræk, G.; Achmann, F.L. Overall size of mannuronan C5-Epimerases influences their ability to epimerize modified alginates and alginate gels. *Carbohydr. Polym.* **2018**, *180*, 256–263. [[CrossRef](#)] [[PubMed](#)]
46. Draget, K.I.; Smidsrød, O.; Skjåk-Bræk, G. Alginates from Algae. In *Biopolymers, Biology, Chemistry, Biotechnology, Applications*; Alexander, S., Ed.; Wiley: Hoboken, NJ, USA, 2005; Volume 1, ISBN 9783527600038.
47. Jain, S.; Mondal, K.; Gupta, M.N. Applications of Alginate in Bioseparation of Proteins Applications of Alginate in Bioseparation of Proteins. *Artif. Cells Blood Substit. Biotechnol.* **2006**, *34*, 127–144. [[CrossRef](#)] [[PubMed](#)]
48. Usov, A.I.; Smirnova, G.P.; Kamenarska, Z.; Dimitrova-konaklieva, S. Polar Constituents of Brown Seaweed *Colpomenia peregrina* (Sauv.) Hamel from the Black Sea. *Russ. J. Bioorganic Chem.* **2004**, *30*, 161–167. [[CrossRef](#)] [[PubMed](#)]
49. Đorović, J.; Marković, Z.; Petrović, Z.D.; Simijonović, D.; Petrović, V.P. Theoretical analysis of the experimental UV-Vis absorption spectra of some phenolic schiff bases. *Mol. Phys.* **2017**, *115*, 2460–2468. [[CrossRef](#)]
50. Sathya, R.; Kanaga, N.; Sankar, P.; Jeeva, S. Antioxidant properties of phlorotannins from brown seaweed *Cystoseira trinodis* (Forsskål) C. Agardh. *Arab. J. Chem.* **2017**, *10*, S2608–S2614. [[CrossRef](#)]
51. Antosiewicz, J.M.; Shugar, D. UV-Vis spectroscopy of tyrosine side-groups in studies of protein structure. Part 1: Basic principles and properties of tyrosine chromophore. *Biophys. Rev.* **2016**, *8*, 151–161. [[CrossRef](#)]
52. Pawar, S.N.; Edgar, K.J. Alginate derivatization: A review of chemistry, properties and applications. *Biomaterials* **2012**, *33*, 3279–3305. [[CrossRef](#)]
53. Salomonsen, T.; Jensen, H.M.; Larsen, F.H.; Steuernagel, S.; Engelsen, S.B. Direct quantification of M/G ratio from <sup>13</sup>C CP-MAS NMR spectra of alginate powders by multivariate curve resolution. *Carbohydr. Res.* **2009**, *344*, 2014–2022. [[CrossRef](#)]
54. Grasdalen, H. High-field, 1H-n.m.r. spectroscopy of alginate: Sequential structure and linkage conformations. *Carbohydr. Res.* **1983**, *118*, 255–260. [[CrossRef](#)]

55. Penman, A.; Sanderson, G.R. A method for the determination of uronic acid sequence in alginates. *Carbohydr. Res.* **1972**, *25*, 273–282. [[CrossRef](#)]
56. Khanna, O.; Moya, M.L.; Opara, E.C.; Brey, E.M. Synthesis of multilayered alginate microcapsules for the sustained release of fibroblast growth factor-1. *J. Biomed. Mater. Res. Part A* **2010**, *95*, 632–640. [[CrossRef](#)] [[PubMed](#)]
57. Wang, Q.; Nielsen, U.G. Applications of solid-state NMR spectroscopy in environmental science. *Solid State Nucl. Magn. Reson.* **2020**, *110*, 101698. [[CrossRef](#)] [[PubMed](#)]
58. Cardenas-Jiron, G.; Leal, D.; Matsuiro, B.; Osorio-Roman, I.O. Vibrational spectroscopy and density functional theory calculations of poly-D-mannuronate and heteropolymeric fractions from sodium alginate. *J. Raman Spectrosc.* **2011**, *42*, 870–878. [[CrossRef](#)]
59. Leal, D.; Matsuiro, B.; Rossi, M.; Caruso, F. FT-IR spectra of alginic acid block fractions in three species of brown seaweeds. *Carbohydr. Res.* **2008**, *343*, 308–316. [[CrossRef](#)] [[PubMed](#)]
60. Maddams, W.F.; Mead, W.L. The measurement of derivative i.r. spectra-I. Background studies. *Spectrochim. Acta Part A Mol. Spectrosc.* **1982**, *38*, 437–444. [[CrossRef](#)]
61. Martínez-Gómez, F.; Mansilla, A.; Matsuiro, B.; Matulewicz, M.C.; Troncoso-Valenzuela, M.A. Chiroptical characterization of homopolymeric block fractions in alginates. *Carbohydr. Polym.* **2016**, *146*, 90–101. [[CrossRef](#)]
62. Martínez-Gómez, F.; Encinas, M.V.; Matsuiro, B.; Pavez, J. Preparation and swelling properties of homopolymeric alginic acid fractions/poly(N-isopropyl acrylamide) graft copolymers. *J. Appl. Polym. Sci.* **2015**, *132*, 1–10. [[CrossRef](#)]
63. Kristiansen, K.A.; Tomren, H.B.; Christensen, B.E. Periodate oxidized alginates: Depolymerization kinetics. *Carbohydr. Polym.* **2011**, *86*, 1595–1601. [[CrossRef](#)]
64. Vishratina, A.K.; Purcell-Milton, F.; Serrano-García, R.; Kuznetsova, V.A.; Orlova, A.O.; Fedorov, A.V.; Baranov, A.V.; Gun'ko, Y.K. Chiral recognition of optically active CoFe<sub>2</sub>O<sub>4</sub> magnetic nanoparticles by CdSe/CdS quantum dots stabilised with chiral ligands. *J. Mater. Chem. C* **2017**, *5*, 1692–1698. [[CrossRef](#)]
65. Larsen, B.; Painter, T.J. Preliminary communication the periodate-oxidation limit of alginate. *Carbohydr. Res.* **1969**, *10*, 186–187. [[CrossRef](#)]
66. Córdova, B.M.; Jacinto, C.R.; Alarcón, H.; Mejía, I.M.; López, R.C.; de Silva, D.O.; Cavalheiro, E.; Venâncio, T.; Dávalos, J.Z.; Valderrama, A.C. Chemical modification of sodium alginate with thiosemicarbazide for the removal of Pb(II) and Cd(II) from aqueous solutions. *Int. J. Biol. Macromol.* **2018**, *120*, 2259–2270. [[CrossRef](#)] [[PubMed](#)]
67. Kallen, R.G. Equilibria for the Reaction of Cysteine and Derivatives with Formaldehyde and Protons. *J. Am. Chem. Soc.* **1971**, *93*, 6227–6235. [[CrossRef](#)] [[PubMed](#)]
68. Smidsrød, O.; Larsen, B.; Haug, A. Acid hydrolysis of polysaccharides containing uronic acid residues. *Carbohydr. Res.* **1967**, *5*, 371–372. [[CrossRef](#)]
69. Kristiansen, K.A.; Dalheim, M.; Christensen, B.E. Periodate oxidation and macromolecular compaction of hyaluronan. *Pure Appl. Chem.* **2013**, *85*, 1893–1900. [[CrossRef](#)]
70. Alinezhad, H.; Tajbakhsh, M.; Hamidi, N. Reductive amination of aldehydes and ketones using sodium borohydride in the presence of silica chloride under solvent-free conditions. *Chin. Chem. Lett.* **2010**, *21*, 47–50. [[CrossRef](#)]
71. Cho, B.T.; Kang, S.K. Direct and indirect reductive amination of aldehydes and ketones with solid acid-activated sodium borohydride under solvent-free conditions. *Tetrahedron* **2005**, *61*, 5725–5734. [[CrossRef](#)]
72. Kumar, N.U.; Reddy, B.S.; Reddy, V.P.; Bandichhor, R. Iron triflate catalyzed reductive amination of aldehydes using sodium borohydride. *Tetrahedron Lett.* **2012**, *53*, 4354–4356. [[CrossRef](#)]
73. Saberi, D.; Akbari, J.; Mahdudi, S.; Heydari, A. Reductive amination of aldehydes and ketones catalyzed by deep eutectic solvent using sodium borohydride as a reducing agent. *J. Mol. Liq.* **2014**, *196*, 208–210. [[CrossRef](#)]
74. Reddy, P.S.; Kanjilal, S.; Sunitha, S.; Prasad, R.B.N. Reductive amination of carbonyl compounds using NaBH<sub>4</sub> in a Brønsted acidic ionic liquid. *Tetrahedron Lett.* **2007**, *48*, 8807–8810. [[CrossRef](#)]